Non-Double-Couple Earthquakes in the Long Valley Volcanic Region

by Dennise C. Templeton and Douglas S. Dreger

Abstract   To better understand the connection between earthquake production and geothermal/magmatic systems, we studied the extent of fluid-influenced faulting in the Long Valley volcanic region. We focused on a 100-km-wide circular area centered at the Long Valley caldera that also encompassed the Mono-Inyo craters to the north and the Sierra Nevada mountain block to the south. We performed a comprehensive search for events greater than M 3.5 since 1993 with significant coseismic volume changes in their source region. Using three-component broadband digital waveforms at regional distances, we solved for four different source models: double couple (DC), deviatoric DC + isotropic, and full moment tensor. Using the F-test as a statistical aid, we determined which of the four models was most appropriate for each event. We then conducted stability tests to determine the robustness of the focal mechanism solutions and isotropic components. Our results show that fluid-influenced earthquakes in the magnitude range studied are quite rare in the Long Valley volcanic region. Of 33 high-quality events, 28 are best characterized by a simple DC source model, 4 by a DC + isotropic source model, and 1 by a full moment tensor model.

Introduction

In volcanic areas, deviations from the usual double-couple (DC) model of shear faulting may be able to illuminate a link between the source process of an earthquake and fluids associated with the geothermal or magmatic system. These non-DC earthquakes have mechanisms vastly different from simple shear along a planar fault and are characterized by a compensated-linear-vector-dipole (CLVD) component, suggesting either fluid involvement or complex shear failure, and/or an isotropic component that describes volume changes in the source region. Many possible physical mechanisms have been proposed to account for these two non-DC components; however, the details of these physical source processes are still not well understood (Julian *et al.*, 1998).

Non-DC events with significant volumetric components have been observed in various volcanic and geothermal areas such as The Geysers geothermal area, California; Aso Volcano, Japan; and Mt. Etna and Campi Flegrei, Italy (Ross *et al.*, 1999; Legrand *et al.*, 2000; Saraò *et al.*, 2001; Guidarelli *et al.*, 2002). These studies have shown that the percentage of events with isotropic components and the strength of the isotropic component can vary with location. These differences appear to be due to different underlying physical mechanisms. Four non-DC events have also been previously identified in the Long Valley caldera, California (Dreger *et al.*, 2000). In this article, we consider the Long Valley caldera along with the Mono-Inyo craters and the seismically active Sierra Nevada block to be part of the Long Valley volcanic region located in eastern California within the Sierra Nevada frontal fault system (Fig. 1).

Since the installation of geophysical monitoring equipment, Long Valley caldera has displayed periods of unrest characterized by increased seismicity, ground deformation, localized increases in volcanic gas emissions, and subsurface magma movement. The most recent episode of unrest within the caldera began in 1997 with progressively increasing deformation rates across the resurgent dome followed by an increase in the rate of earthquake production in the south moat of the caldera (Hill *et al.*, 2003). Well water-level changes due to local large earthquakes associated with this swarm have been attributed to the upward migration of high-temperature fluids beneath the south moat of the caldera (Roeloffs *et al.*, 2003). Surface deformation within the caldera over this time period has been modeled using two deep magmatic inflation sources, one 6–7 km below the resurgent dome and another 10–20 km below the south moat of the caldera combined with right-lateral slip on a steeply dipping plane in the south moat (Langbein, 2003). This modeling is consistent with previous seismic studies using S-to-P amplitude ratios, teleseismic P-wave polarizations, and P_s converted waves that have mapped an anomalous region 7–12 km below the resurgent dome, indicating a high-temperature region containing an area with a significant percentage of melt and the top of the offset central magma body (Steck and Prothero, 1994; Sanders and Nixon, 1995).

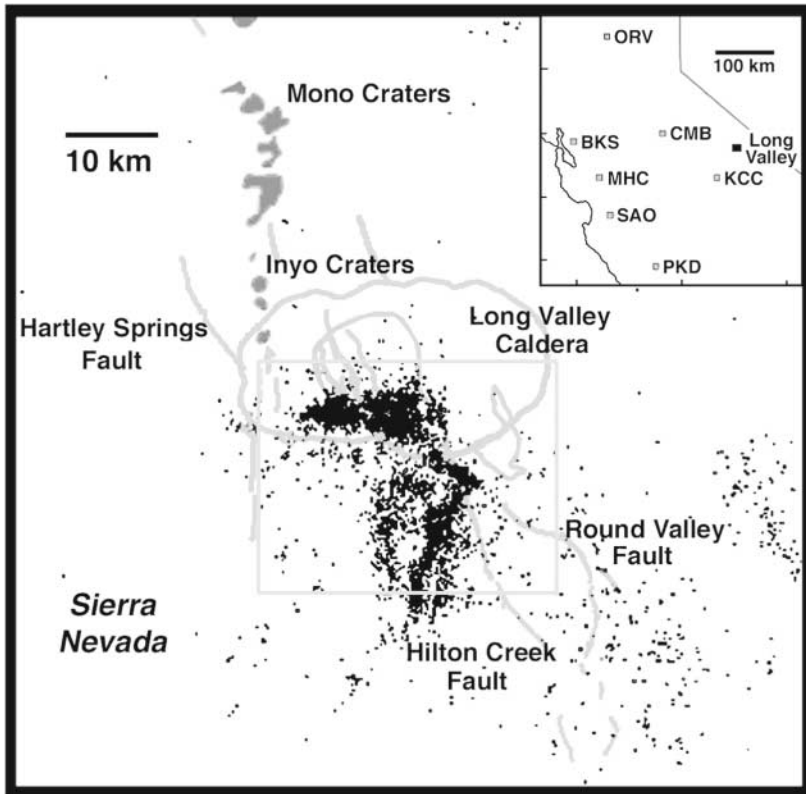Equivocal evidence for fluids has also been identified

Figure 1. Area map showing location of the Long Valley caldera, Mono-Inyo volcanic chain, and major Sierra Nevada frontal faults. Northern California Seismic Network (NCSN) catalog seismicity between 1980 and 2000 shown as small gray dots. Inset map of California shows the distribution of stations used in this study. Rectangle delineates area plotted in Figure 2.

south of the caldera in the seismically active Sierra Nevada block. Three large events, the M 5.8 4 October 1978 Wheeler Crest earthquake along with two May 1980 events greater than M 6, were best described using a combination of DC and CLVD components (Julian and Sipkin, 1985). Unlike the 1978 event, the 1980 earthquakes were part of a larger earthquake swarm that extended up into the Long Valley caldera. The CLVD components were thought to be due to water or low-viscosity magma involvement in the source process. However, there has been much controversy surrounding this solution, since these events can also be modeled using a complex DC source involving multiple rupture planes (Wallace, 1985). Unfortunately, the exact source model cannot be resolved with the available data, and this controversy continues. Additionally, in August 1998, during a minor earthquake sequence without a clear mainshock, three microearthquakes displayed strikingly harmonic spectral signatures that were hypothesized to have been caused by a magmatic-fluid-controlled source process (Hough *et al.*, 2000). Possible magma bodies have also been identified in the Sierra Nevada block from early *S*-wave shadowing studies (Ryall and Ryall, 1984). In contrast to the caldera and the Sierra Nevada block, the Mono-Inyo volcanic chain to the north has exhibited little seismicity even though the most recent volcanic eruption occurred in this region (Sieh, 1984).

In this study, we investigated the source mechanisms of events greater than M 3.5 occurring between 1993 and 2003 within a 100-km-wide circular area centered at the Long

Valley caldera to identify events with significant coseismic volume changes. In this active geothermal and magmatic area, we treat coseismic volume changes as an indicator of fluid involvement at the source. Our results show that events with significant volumetric components in this magnitude range were fairly rare over the observation period. Of 33 high-quality events, 28 are best characterized by a simple DC source model, and only 5 have coseismic volume increases.

Data and Methodology

In this study we solved for four different source models: DC, deviatoric (DC + CLVD), DC + isotropic, and the full moment tensor model. In our analysis, the full moment tensor solution is decomposed into deviatoric and volumetric components. The deviatoric portion is then further decomposed into DC and CLVD components by assuming that the same principal stresses produced both components, thus allowing for the inclusion of DC, CLVD, and volumetric forces in the source process. This model can characterize source processes involving a combination of tensile and shear faulting (Julian *et al.*, 1998). The deviatoric moment tensor solution *a priori* sets the volumetric component to zero, and solves only for the DC and CLVD components. This model describes volume-conserving source processes that deviate from a simple DC mechanism. DC + isotropic source mechanisms have been used to describe combinations of near-

simultaneous faulting near an underground explosion source (Massé, 1981; Dreger and Woods, 2002). The pure DC model assumes that the earthquake source is best modeled as shear along a planar fault and *a priori* sets the CLVD and volumetric components to zero.

For the DC and DC + isotropic models, a grid-search method iterating over strike, dip, rake, DC moment, and isotropic moment, which is equal to zero in the pure DC case, was used to find the solution that best fit the observed three-component waveforms bandpass filtered between 0.02 and 0.05 Hz. Since the grid-search method finely searched over the entire model space, we feel confident that although the method iterates over nonlinear equations, it does not suffer from local minima complications such as those common in linearized approaches. For the deviatoric and full moment tensor models, the second-rank symmetric seismic moment tensor is solved by linearly inverting complete three-component filtered broadband seismograms in the time domain using a weighted least-squares approach. The percent isotropic for these models is determined by dividing the isotropic moment, one-third the trace of the diagonalized moment tensor, by the total moment. The deviation of the source from a DC is determined by $\varepsilon = |\lambda_{\min}/\lambda_{\max}|$, where $\lambda_{\min}$ and $\lambda_{\max}$ refer to the smallest and largest eigenvalues in an absolute sense. The percent DC and CLVD of the deviatoric portion of the moment tensor is then $(1 - 2\varepsilon) \times 100\%$ and $(2\varepsilon) \times 100\%$, respectively. Green's functions for all four models were computed utilizing a frequency-wavenumber integration method and the SoCal velocity model (Dreger and Helmberger, 1993) for source depths every 3 km between 2 and 17 km. A set of seven Berkeley Digital Seismic Network stations (BKS, CMB, KCC, MHC, ORV, PKD, and SAO) providing the best azimuthal coverage and data quality are used in this investigation. In practice, however, a solution would usually have a subset of these stations depending on station availability and data-quality issues.

The variance reduction is the goodness-of-fit parameter between the data and synthetics and is computed using

$$\text{VR} = \left(1 - \frac{\int (d - s)^2 dt}{\int d^2 dt}\right) \times 100\%$$

where *d* refers to the data and *s* to the synthetics, with implied time dependence. A variance reduction of 100% would indicate an exact match between the data and synthetics. This measure was used to assess the quality of each of the solutions. Best depths were determined by choosing the solution with the highest variance reduction in the range of possible depths determined by the extensive Northern California Seismic Network.

When testing more complex source models, the variance reduction usually increases with increasing complexity. *F*-test statistics were performed to determine if the additional CLVD and/or volumetric components represented a true as-

pect of the source mechanism or if they simply added non-physical parameters to the inversion. To do this we computed the prediction error, e_i,

$$e_i = (d_i - s_i)$$

where *d* and *s* are the data and synthetics at a particular time *i*, to estimate the variance, σ^2,

$$\sigma^2 = \frac{\sum e_i}{(N - M)}$$

of each model where *N* and *M* are the number of observations and model parameters. For the DC, deviatoric, DC + isotropic, and full moment tensor (FMT) models there are four, five, five, and six independent model parameters, respectively. The number of observations are the number of uncorrelated data points per waveform multiplied by the number of waveforms used in the inversion. For waveforms bandpass filtered between 0.02 and 0.05 Hz, the number of uncorrelated data points for a 200-sec waveform is set to 10 assuming 1 sample/sec and a 20-sec width for the lowpass filter corner. The *F*-test statistic is determined by taking the ratio of the variances

$$F \text{ ratio } 1 = \frac{\sigma_{DC}^2}{\sigma_{\text{dev}}^2}$$

$$F \text{ ratio } 2 = \frac{\sigma_{DC+\text{isotropic}}^2}{\sigma_{\text{FMT}}^2}$$

$$F \text{ ratio } 3 = \frac{\sigma_{DC}^2}{\sigma_{DC+\text{isotropic}}^2}$$

$$F \text{ ratio } 4 = \frac{\sigma_{\text{dev}}^2}{\sigma_{\text{FMT}}^2}$$

and comparing these values with known statistical tables. The degrees of freedom for each model is equal to $N - M - 1$ (Menke, 1989). In this way we tested whether the more complex model fit the data significantly better than the simpler model. We determined that the more complex model was appropriate if the improvement in fit to the data was at or above the 95% confidence level as dictated by the *F*-test. By taking all four *F* ratios into account it becomes clear whether any, either, or both non-DC components are significant.

Results

Within the chosen space and time constraints, 33 high-quality events are identified that have solutions with three or more stations in their inversion (Table 1). Of these 33 events, 28 are best characterized using a simple DC model.

Synthetic waveforms produced using the more complex source models do not fit the data significantly better. This is quantitatively determined using the four statistical tests that show that the deviatoric, DC + isotropic, and full moment tensor model waveforms do not significantly improve the solution at or above the 95% confidence level using an F test. Table 2 gives the derived focal mechanism solutions for these 28 DC events.

The remaining five events all have statistically significant positive volumetric components. The two statistical tests that determine the significance of the volumetric components, F ratios 3 and 4, show that source models containing isotropic components fit the data significantly better than source models that do not. For these five events, we use F ratio 2 to determine if the CLVD component is also significant. This test shows that only one of the five, event 10, also has a statistically significant CLVD component. Tables 3 and 4 show the mechanisms for the DC + isotropic and full moment tensor events, respectively. The variance reduction values in Table 5 show how well each model fits the waveforms of the non-DC events. Table 6 gives the results of the

F-tests for the five events with significant volumetric components. Assuming that both F ratios 3 and 4 determine that an event does not have a statistically significant isotropic component, F ratio 1 can determine if a deviatoric source model is preferred over a DC source model. However, none of the 33 events are best characterized by a deviatoric source model. At this point, it is important to remember that the applied statistics can only determine which of the four source models is most appropriate for each earthquake, but place no guarantee on the physical mechanism behind these non-DC events. All non-DC events are located either in the south moat of the caldera or in the Sierra Nevada block (Fig. 2). We were not able to analyze the source process of earthquakes in or near the vicinity of the Mono-Inyo volcanic chain or Mammoth Mountain because events greater than M 3.5 were not recorded during the time interval investigated by this study.

The first event with a significant volumetric component, event 1, occurred on 11 August 1993 in the Sierra Nevada block during an intense earthquake swarm. The six-day Red Slate Mountain earthquake swarm started on 10 August and

Table 1
List of Events

Event	UTC Date (yyyy/mm/dd)	UTC Time (hh:mm:ss)	Latitude North	Longitude West	NCSN Magnitude	Depth (km)
1	1993/08/11	05:48:20.94	37.5262	−118.8835	4.3	5.13 ± 1.01
2	1995/03/05	00:07:03.12	37.5975	−118.8325	4.2	10.34 ± 0.55
3	1995/03/05	02:48:47.42	37.5928	−118.8325	4.0	10.56 ± 0.54
4	1996/02/17	01:03:48.29	37.6240	−118.8758	3.6	8.73 ± 0.37
5	1996/03/29	18:14:49.42	37.6293	−118.8530	3.9	8.92 ± 0.43
6	1996/03/30	23:15:18.50	37.6282	−118.8657	4.0	7.54 ± 0.36
7	1996/04/01	04:13:36.49	37.6178	−118.8568	3.9	9.78 ± 0.38
8	1996/04/02	01:50:07.61	37.6243	−118.8610	4.2	7.98 ± 0.37
9	1997/02/10	23:26:28.88	37.5648	−118.8605	4.2	9.76 ± 0.85
10	1997/11/22	12:06:55.98	37.6352	−118.9175	4.5	8.38 ± 0.35
11	1997/11/22	17:20:35.14	37.6363	−118.9360	4.8	7.66 ± 0.38
12	1997/11/22	18:00:37.44	37.6445	−118.9492	3.5	7.96 ± 0.73
13	1997/11/22	18:10:59.45	37.6340	−118.9507	4.7	8.20 ± 0.34
14	1997/11/30	21:17:05.42	37.6343	−118.9462	4.8	7.10 ± 0.45
15	1997/12/31	20:36:47.34	37.6312	−118.8697	4.8	6.59 ± 0.32
16	1998/01/05	14:11:12.89	37.6338	−118.8712	4.1	6.43 ± 0.35
17	1998/06/08	03:55:14.43	37.5893	−118.7975	4.0	6.66 ± 0.50
18	1998/06/09	05:24:40.16	37.5887	−118.7955	5.1	6.75 ± 0.48
19	1998/06/11	06:33:29.08	37.5842	−118.7843	4.3	8.26 ± 0.53
20	1998/06/26	20:07:41.85	37.5925	−118.8070	4.3	6.21 ± 0.46
21	1998/07/15	04:53:19.25	37.5635	−118.8063	5.1	6.22 ± 0.55
22	1998/07/15	06:50:56.89	37.6440	−118.9123	3.7	7.14 ± 0.32
23	1998/08/01	06:01:43.96	37.5693	−118.7935	4.3	5.93 ± 0.73
24	1998/08/02	14:45:45.47	37.5725	−118.7972	4.3	6.79 ± 0.51
25	1998/09/11	14:38:42.66	37.3880	−118.6893	3.9	12.30 ± 0.93
26	1998/12/14	04:14:02.94	37.5262	−118.7958	3.8	7.96 ± 2.29
27	1999/05/15	13:22:10.66	37.5298	−118.8172	5.6	5.59 ± 0.56
28	1999/05/15	17:54:08.77	37.5093	−118.8310	4.7	7.33 ± 0.80
29	1999/05/17	06:37:19.15	37.5118	−118.8263	4.3	3.27 ± 0.81
30	1999/05/26	03:53:53.45	37.5558	−118.8035	4.2	4.47 ± 0.65
31	1999/05/26	18:04:07.21	37.5455	−118.8062	4.2	4.09 ± 0.70
32	1999/06/03	21:36:27.74	37.5375	−118.8052	4.4	3.29 ± 0.87
33	2003/03/08	15:35:01.71	37.5705	−118.8848	4.0	5.46 ± 0.34

UTC event date and time. NCSN location, magnitude, and depths, including formal vertical errors.

Table 2
Table of DC Solutions

Event	Stations	MT Depth	Strike	Rake	Dip	M_0	M_w
2	BCO	11	105	−159	78	2.05E+22	4.2
3	BCS	11	357	−24	78	1.16E+22	4.0
4	BCK	8	306	−147	48	6.46E+21	3.8
5	BCKO	8	291	−147	57	8.20E+21	3.9
6	BCKO	8	204	−39	84	3.08E+22	4.3
7	CKO	8	201	−36	42	1.30E+22	4.0
8	BCKO	8	300	−174	54	4.31E+22	4.4
9	COP	8	54	24	78	2.05E+22	4.2
12	BCK	8	279	−174	45	5.33E+21	3.8
15	BCMOPS	5	288	177	51	1.78E+23	4.8
16	BCOP	5	29	27	68	2.07E+22	4.2
17	CKO	8	201	−27	81	3.61E+21	3.7
18	BKMOPS	5	300	177	54	2.85E+23	4.9
19	BCO	8	114	−150	72	8.20E+21	3.9
20	BCO	5	33	9	69	1.03E+22	4.0
21	BCKMOPS	5	165	−87	45	3.08E+23	5.0
22	BCK	8	270	−171	42	5.13E+21	3.8
23	BCOP	5	123	−156	81	1.78E+22	4.1
24	CKOP	5	324	−129	42	1.46E+22	4.1
25	BOPS	14	69	6	78	6.65E+21	3.9
26	CKO	5	120	−174	72	6.46E+21	3.8
27	BMOPS	5	294	−171	72	2.32E+24	5.5
28	BKOP	8	291	−177	57	1.05E+23	4.7
29	CKO	2	327	−129	51	8.61E+21	3.9
30	BMOPS	5	15	−18	63	9.90E+21	4.0
31	CKO	5	105	−159	78	5.38E+21	3.8
32	BKO	2	6	−18	42	3.61E+22	4.3
33	BCKMO	5	3	−39	54	1.44E+22	4.1

Station code is B = BKS, C = CMB, K = KCC, M = MHC, C = ORV, P = PKD, and S = SAO.

Table 3
Table of DC + Isotropic Solutions

Event	Stations	MT Depth	Strike	Rake	Dip	DC M_0	ISO M_0	M_w
1	BCO	5	108	156	48	1.91E+22	1.76E+22	4.2
11	BCMOPS	8	24	48	63	2.49E+23	1.32E+23	4.9
13	BCMOS	8	342	18	75	6.67E+22	3.84E+22	4.5
14	BCKMOS	8	18	27	60	2.41E+23	9.50E+22	4.9

Station code is B = BKS, C = CMB, K = KCC, M = MHC, O = ORV, P = PKD, and S = SAO.

Table 4
Table of Full Moment Tensor Solutions

Event	Stations	MT Depth	M_{xx}	M_{xy}	M_{xz}	M_{yy}	M_{yz}	M_{zz}	M_w
10	BCMOS	8	4.7567	3.9713	−5.1655	4.0490	−4.7136	6.3743	4.5

Moment tensor components have units of 10^{22} dyne cm. Station code is B = BKS, C = CMB, M = MHC, O = ORV, and S = SAO.

Table 5
Variance Reduction of All Four Source Models for Non-DC Events

Event	DC VR	Deviatoric VR	DC+Iso VR	FMT VR
1	88.2%	88.5%	92.4%	93.4%
10	79.3%	83.2%	85.5%	89.1%
11	83.1%	86.3%	90.8%	92.0%
13	82.1%	88.4%	91.2%	91.8%
14	84.8%	85.9%	89.0%	91.0%

VR, variance reduction; DC+Iso, DC + isotropic; FMT, full moment tensor.

F ratio 2 determines that adding the CLVD component to the inversion does not significantly improve the solution. Hence, the best source model for this event is the DC + isotropic model. The isotropic component of this event contributes 48% of the total moment release.

The next four events with coseismic volume increases (events 10, 11, 13, and 14) occurred in the south moat of the Long Valley caldera during a period of unrest at the peak of a large earthquake swarm that spanned July 1997 though January 1998. These events had been previously identified as having significant volumetric components by Dreger *et al.* (2000); however, the current study investigates a wider range of possible source mechanisms. Thus, the results pre-

produced the largest earthquake and the greatest number of events associated with a single earthquake swarm in the Long Valley volcanic region in 1993. As seen in Table 6, F ratios 3 and 4 determine that this event has a statistically significant isotropic component at the 95% confidence level.

sented here update the solutions of the previous investigation. We will first discuss event 10. Both F ratios 3 and 4 indicate that this event has a significant isotropic component. We then utilized F ratio 2, since it *a priori* assumes that the event in question has a significant isotropic component, to determine if the CLVD component is also significant. The results of this test indicate that the addition of the CLVD component significantly improves the fit to the data. As such, event 10 is best described using the full moment tensor model. The CLVD component of this event contributes a large 57% to the total moment release while the isotropic component contributes 42%. Interestingly, the DC component is only 1% of the total moment, suggesting that shear along a fault plane was not an important part of the earthquake process and implying that the mechanism for this event resembled an opening tensile fault.

For event 11, both F ratios 3 and 4 indicate that this earthquake has a significant isotropic component at the 99% confidence level. The results of F ratio 2 indicate that the CLVD component is statistically insignificant. Hence, this event is best described using the DC + isotropic model. This solution revealed that the isotropic component produced 35% of the total moment release for this event. As an example of how the different sources can influence the waveforms, Figure 3 compares the filtered data observed at station SAO with synthetic waveforms computed using the four different source models. In this example, the most notable differences can be seen in the radial component. Figure 4 compares the observed data at all stations for event 11 with the DC + isotropic source synthetic waveforms.

For event 13, F tests 3 and 4 also indicate that this event has a significant isotropic component while F ratio 2 determines that this event has a statistically insignificant CLVD component. Thus, this event is also best modeled using the DC + isotropic solution. The results of this inversion indicate that the isotropic component of this event contributes 27% of the total moment release.

Table 6
Greater than 95% Significance Levels for Non-DC Events

Event	F ratio 1 DC vs. Dev	F ratio 2 DC + Iso vs. FMT	F ratio 3 DC vs. DC + Iso	F ratio 4 Dev vs. FMT	Best Mechanism
1	—	—	95%	95%	DC + iso
10	—	95%	95%	99%	FMT
11	—	—	99%	99%	DC + iso
13	99%	—	99%	95%	DC + iso
14	—	—	95%	99%	DC + iso

F ratios 1 and 2 test for significant CLVD components. F ratios 3 and 4 test for significant isotropic components. Dev, deviatoric; DC + Iso, DC + isotropic; FMT, full moment tensor.
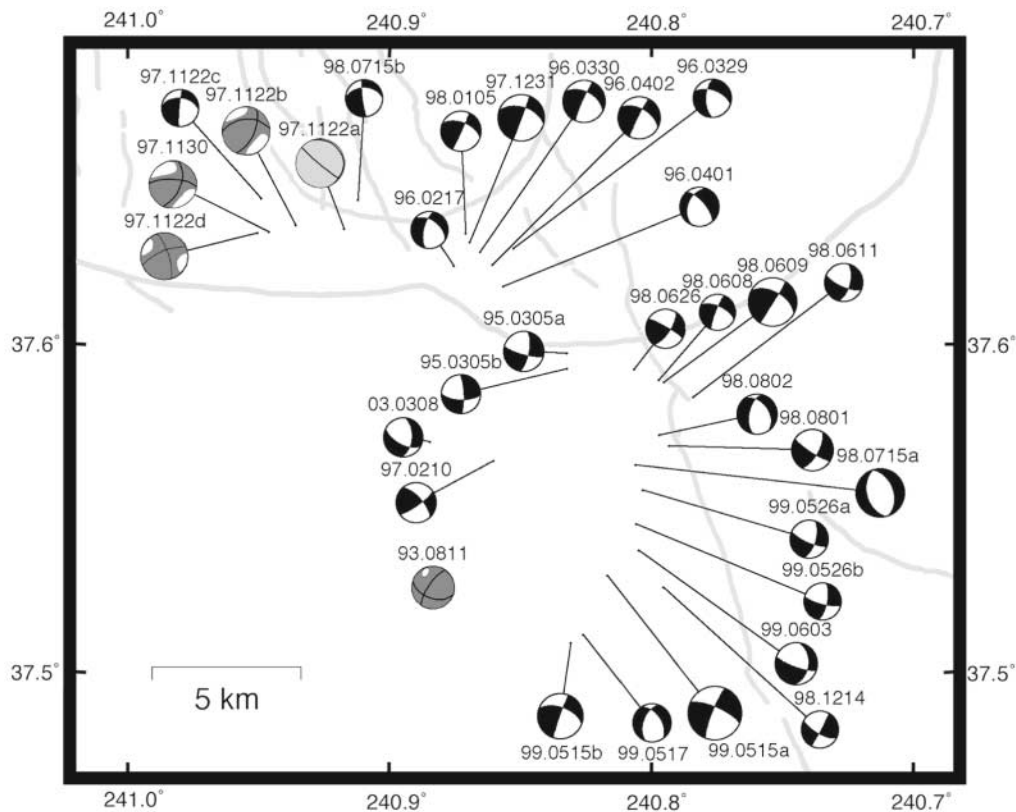

Figure 2. Graphical moment tensor results. DC solutions shown in black. DC + isotropic solutions shown as dark gray. Full moment tensor solutions shown as light gray. Date of event shown as YY.MMDD.
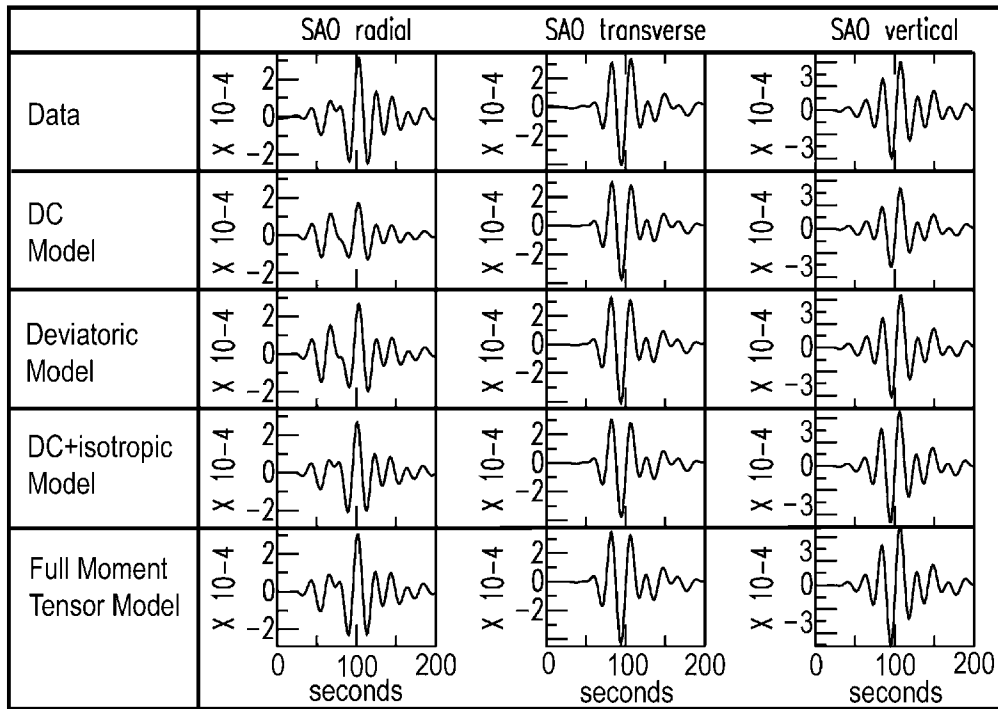
Figure 3.   Data, DC model synthetics, deviatoric model synthetics, DC + isotropic model synthetics, and full moment tensor model synthetics filtered between 0.02 and 0.05 Hz for all three components at station SAO for DC + isotropic event 11 in units of centimeters.

For the remaining event, event 14, *F* tests 3 and 4 again indicate that it has a significant isotropic component. As seen in Table 6, *F* ratio 2 indicates that this event does not have a significant CLVD component. As such, this event is best modeled using the DC + isotropic source model. The isotropic component of event 14 contributes 35% of the total moment.

Pure DC events sometimes occurred close in space and time to events with significant non-DC components (Fig. 2). For example, DC event 12 occurred 10 minutes before non-DC event 13 and was located just a few kilometers away from all four south-moat non-DC events. In some cases, DC events determined by this study were located near previously identified fluid-influenced microseismicity structures. For example, events 15 and 16 occurred close in space to a microseismicity trend inferred to be a compensated tensile failure plane (Foulger *et al.*, 2004). Thus, it appears that the factors necessary to produce isotropic components only coalesce and trigger non-DC events within a relatively small physical and temporal window in the Long Valley volcanic region.

Stability of Focal Mechanism Solutions

To test the stability of the focal mechanism solution, we performed jackknife tests on three events: DC event 15, DC + isotropic event 11, and full moment tensor event 10. We solved for all combinations of three, four, and five station

combinations and compared these results with the original solution for each event. In Figure 5, we show a representative set of focal mechanisms showing the distribution of calculated solutions. DC and DC + isotropic solutions are remarkably stable for all station combinations of three or more. The full moment tensor event shows that the *P*-wave radiation pattern is stable with at least four stations in the inversion but that the orientation of the faulting planes is unstable regardless of the number of stations used. However, it is important to note that the DC component of this event produced only 1% of the total moment release and that the CLVD and isotropic components dominate the inversion; hence the instability of the faulting planes is not surprising. Most of the three station inversions produced similar radiation patterns to solutions using more stations; however, there were a few exceptions (Fig. 5). Thus, focal mechanism solutions with as few as three stations can be treated with confidence. This is consistent with previous stability studies in other volcanic areas (Šílený *et al.*, 1996; Panza and Saraò, 2000).

Stability of the Isotropic Component

Previous studies of synthetic and real data recorded at local distances have investigated how noise, hypocenter mislocation, and velocity-model inaccuracies affect the resolution of the isotropic component, taking into account the distribution of seismic stations (Šílený *et al.*, 1996; Panza and
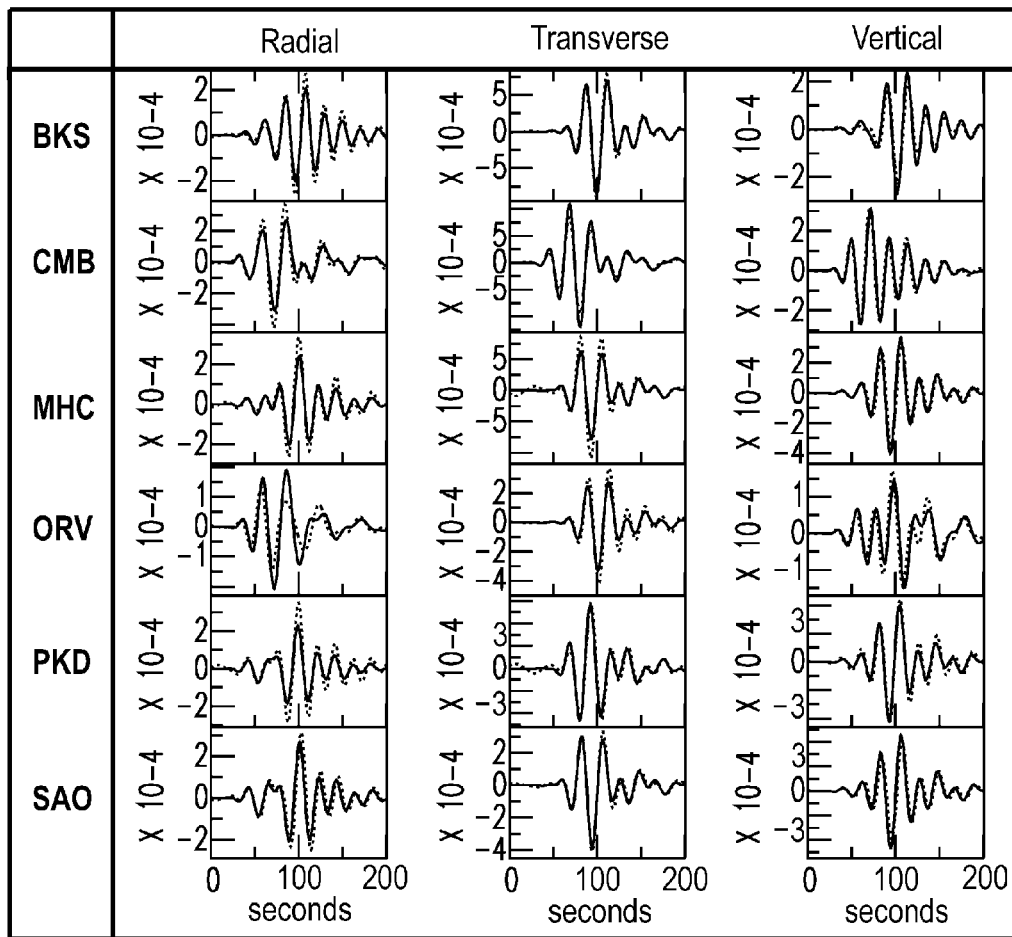
Figure 4.   Best solution for event 11 showing data in dotted black lines and DC +
isotropic model synthetics in solid black lines in units of centimeters.
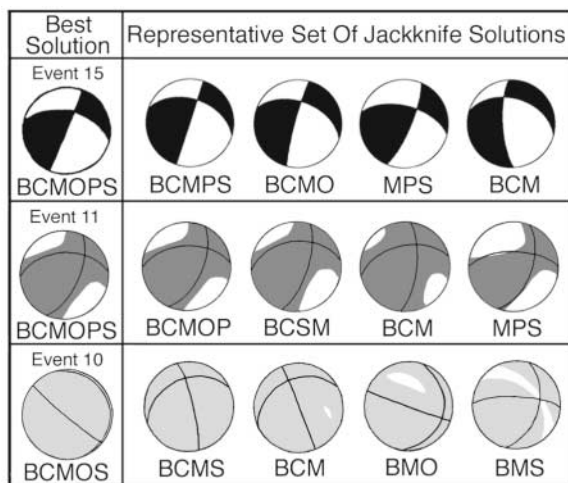

Figure 5.   A representative set of focal mechanism
solutions of jackknife test results for DC event 15, DC
+ isotropic event 11, and full moment tensor event
10. Station code is B = BKS, C = CMB, M = MHC,
O = ORV, P = PKD, and S = SAO.

Saraò, 2000). The studies using synthetic data have shown
that the isotropic component can be correctly recovered even
with poor station configurations when as few as three three-
component local stations are used. These synthetic tests have
also shown that errors in the hypocenter and velocity model
are small compared to errors due to high noise levels.

In this study, we conducted a detailed investigation of
33 events with low noise levels. With respect to the velocity
model, at the passband used in this study, the SoCal model
has been shown to not produce statistically significant iso-
tropic components due to unmodeled near-source velocity
structure in the Long Valley caldera (Panning *et al.*, 2001).
To determine the stability of the isotropic component with
station configuration for data recorded at regional distances,
we first performed jackknife tests on the four events with
significant isotropic components that had four or more sta-
tions in their solution to determine the likelihood of non-DC
events incorrectly being identified as DC events. Thus, for
each event, for all station combinations of three or more, we
determined the statistical significance of the volumetric com-
ponent. For the event with the significant CLVD component,

event 10, we compared the deviatoric and full moment tensor solutions. For events without significant CLVD components, we compared the DC and DC + isotropic solutions. Statistically significant isotropic components were determined if the improvement in fit to the data was at or above the 95% significance level as determined by using the *F*-test statistic. Unfortunately, event 1 had only three stations with good-quality data and thus jackknife tests were not performed on this event. For events 10 and 13, there were 5 four-station solutions and 10 three-station solutions. For events 11 and 14, there were 6 five-station solutions, 15 four-station solutions, and 20 three-station solutions.

All 52 combinations of four or more stations recovered the statistically significant isotropic component. For solutions with three stations, 6 iterations out of 60 failed to recover the isotropic component. It is reasonable to assume that significant isotropic components can be recovered with as few as three, but preferably with at least four, stations in the solution.

We also investigated the possibility of obtaining a spurious isotropic component due to poor data coverage. For this test, we took three high-quality DC solutions (events 15, 18, and 21) and performed jackknife tests to see if any combination of three or more stations would result in a statistically significant isotropic component at or above the 95% significance level. For this test we compared the DC and DC + isotropic solutions for all three events. For their best solutions, events 15 and 18 originally had six stations in their solutions, while event 21 had seven stations.

Of 75 three-station solutions, 1 returned a false positive. Of 65 four-station solutions, 3 incorrectly determined that the event had a significant isotropic component. Five- and six-station solutions did not return false positives. Thus, we feel confident that the isotropic components of our non-DC events with at least five stations in their inversion are not due to poor data coverage. This test, however, casts a small amount of doubt as to the validity of non-DC event 1 which has only three stations in its solution.

Discussion

Earthquakes greater than *M* 3.5 with significant non-DC components are not common in the Long Valley volcanic region. Only five such events occurred between 1993 and 2004. Four occurred in the Long Valley caldera during the peak of a large earthquake swarm in November 1997. The remaining event occurred in the seismically active Sierra Nevada block in August 1993 during the largest earthquake swarm that occurred in the area that year. All five had significant isotropic components, indicating that fluids were involved in the source process of these events. No earthquakes occurred in or near the vicinity of the Mono-Inyo craters during the time interval investigated by this study even though the most recent eruption in the region occurred along this volcanic chain and it is the expected location of the

next eruption within the Long Valley volcanic region (Hill *et al.*, 1985).

Of the events that occurred within the caldera, events 11, 13, and 14 are best characterized using a DC + isotropic model, while event 10 is best described using a full moment tensor model that solves for DC, CLVD, and isotropic components. The isotropic components of all four events indicate that there was a coseismic volume increase in the source region. These events occurred during a period of unrest that also affected the geothermal system. Water-level changes at wells within the caldera were attributed to upward migration of hydrothermal fluids (Roeloffs *et al.*, 2003). An examination of relocated seismicity on the day that the four non-DC events occurred revealed a cloud of seismicity that began to migrate at approximately the same time as the first non-DC event occurred (Prejean, 2002). This cloud of seismicity started at approximately 9 km depth and fanned out upward and westward over an approximately 1-km-wide near-vertical fault zone traveling at about 0.05 m/sec for 23 hours to achieve depths as shallow as 4.5 km. This migration is most probably indicative of fluid circulation, which when combined with pre-existing tectonic stresses could have initiated the events with significant isotropic components. In light of the fact that the Long Valley caldera has a known active geothermal system, it is not unexpected to find events with large isotropic components in this area.

Sierra Nevada block event 1 also has a significant non-DC component; however, our solution stability analysis indicated that events with only three stations in their solution have a small chance of producing spurious isotropic components. This study determined that event 1 is best characterized by a DC + isotropic model whose sign indicated a coseismic volume increase in the source region. Since the strike-slip faults in the Sierra Nevada block do not appear to intersect the ring fracture system of the Long Valley caldera (Prejean *et al.*, 2002), we speculate that the source of the fluids influencing event 1 were not geothermal fluids originating from within the caldera that migrated into the Sierra Nevada block via these conduits. Although there has been equivocal evidence of magma or magmatic fluids present in this area from *S*-wave shadowing studies (Ryall and Ryall, 1984) and from the analysis of three microearthquakes observed during an August 1998 earthquake sequence (Hough *et al.*, 2000), the locations of these potential sources of fluids were not near event 1. The most likely potential fluid source would be fluids associated with the local hydrothermal system. Previously, the only non-DC events to occur in this area were a 1978 *M* 5.8 event and two *M* 6 1980 events (Julian and Sipkin, 1985). Event 1, however, did not occur along the same fault planes as these earlier events (Prejean *et al.*, 2002). Additionally, the full six-component moment tensor solution cannot be computed for the three earlier events with the available data, and thus it is not known if the non-DC components were due to fluid involvement or complex shear faulting. In this study, we specifically solved for the full moment tensor and hence can

conclusively rule out complex coseismic shear faulting as a possible mechanism for the five events with significant isotropic components.

The increase of broadband seismometers in geothermal and volcanic areas has facilitated the worldwide exploration for non-DC earthquake source mechanisms. These studies have shown that the percentage of events with isotropic components and the strength of the isotropic component can vary with location. At Aso Volcano, Japan, inversions of near-field broadband signals of long-period tremors and phreatic eruptions have shown primarily isotropic mechanisms, greater than 95% of the total moment released, for dozens of events over a 1-year period (Legrand *et al.*, 2000). Other volcanoes, such as Mt. Etna, produced only 2 microearthquakes out of 28 events with $M \geq 2.0$ with significant volumetric components over a 16-month period preceding the 1991–1993 eruption (Saraò *et al.*, 2001). These volumetric components were between 17% and 47% of the total moment released for each event. A study of 18 microearthquakes occurring during a period of intense seismicity in 1984 at Campi Flegrei showed that less than half of these events had large volumetric components up to 93% of the total moment release (Guidarelli *et al.*, 2002). These differences are most probably due to different underlying physical mechanisms. The Long Valley volcanic area is more similar to the Mt. Etna region in terms of the scarcity and strength of the isotropic components. In this study, out of 33 events investigated, only 5 have significant non-DC mechanisms whose isotropic components are between 27% and 48% of the total moment released for each event.

A previous full moment tensor study using a dense temporary seismic network operating during the summer of 1997 showed that most of 26 microearthquakes less than M 3.1 were characterized by positive CLVD and isotropic components (Foulger *et al.*, 2004). These events, all between 0 and 6 km, were located in the south moat of the caldera, near the southwestern rim of the resurgent dome and under Mammoth Mountain. Foulger *et al.* (2004) determined that the solutions for these microearthquakes were consistent with a combined shear and tensile faulting model with rapid fluid flow into the opening crack. The small magnitude of these events suggests that the fluid involved was probably not magmatic but rather water, steam, or CO_2. Interestingly, five events in that study were equivocally characterized by small volume decreases, indicating a closing of cracks or voids. The difference in the total number of isotropic events in the two magnitude ranges studied in the Long Valley caldera suggests that conditions are scale dependent, possibly in terms of the ability of individual high-pressure reservoirs to sustain pressurization during the faulting process as the crack or fault grows larger. It is interesting to note that events larger than M 3.5 did not occur near the southwestern rim of the resurgent dome or under Mammoth Mountain. Unfortunately, this meant that events in these areas could not be investigated using our method.

The worldwide diversity apparent in the strength and production of isotropic components should be closely studied, ultimately to determine if there is a predictive relationship between these events and changes to the geothermal or magmatic system. To achieve this goal, future studies should strive to combine nonseismic as well as seismic data when determining the source kinematics, the properties of the fluid involved, and the feasibility and physics behind the different possible physical mechanisms.

Data Sources

Acknowledgments

References

Dreger, D. S., and D. V. Helmberger (1993). Determination of source parameters at regional distances with three-component sparse network data, *J. Geophys. Res.* **98,** 8107–8125.

Dreger, D. S., and B. Woods (2002). Regional distance seismic moment tensors of nuclear explosions, *Tectonophysics* **356,** 139–156.

Dreger, D. S., H. Tkalčić, and M. Johnston (2000). Dilational processes accompanying earthquakes in the Long Valley caldera, *Science* **288,** 122–125.

Foulger, G. R., B. R. Julian, D. P. Hill, A. M. Pitt, P. E. Malin, and E. Shalev (2004). Non-double-couple microearthquakes at Long Valley caldera, California, provide evidence for hydraulic fracturing, *J. Volcanol. Geoth. Res.* **132,** 45–71.

Guidarelli, M., A. Saraò, and G. F. Panza (2002). Surface wave tomography and seismic source studies at Campi Flegrei (Italy), *Phys. Earth Planet. Interiors* **134,** 157–173.

Hill, D. P., R. A. Bailey, and A. S. Ryall (1985). Active tectonic and magmatic processes beneath Long Valley caldera, eastern California: an overview, *J. Geophys. Res.* **90,** 11,111–11,120.

Hill, D. P., J. O. Langbein, and S. Prejean (2003). Relations between seismicity and deformation during unrest in the Long Valley caldera, California, from 1995 through 1999, *J. Volcanol. Geot. Res.* **127,** 175–193.

Hough, S. E., R. S. Dollar, and P. Johnson (2000). The 1998 earthquake sequence south of Long Valley caldera, California: hints of magmatic involvement, *Bull. Seism. Soc. Am.* **90,** 752–763.

Julian, B. R., and S. A. Sipkin (1985). Earthquake processes in the Long Valley caldera area, California, *J. Geophys. Res.* **90,** 11,155–11,169.

Julian, B. R., A. D. Miller, and G. R. Foulger (1998). Non-double-couple earthquakes, 2, Theory, *Rev. Geophys.* **36,** 525–549.

Langbein, J. O. (2003). Deformation of the Long Valley caldera, California: inferences from measurements from 1988 to 2001, *J. Volcanol. Geoth. Res.* **127,** 247–267.

Legrand, D., S. Kaneshima, and H. Kawakatsu (2000). Moment tensor analysis of near-field broadband waveforms observed at Aso Volcano, Japan, *J. Volcanol. Geoth. Res.* **101,** 155–169.

Massé, R. P. (1981). Review of seismic source models for underground nuclear explosions, *Bull. Seism. Soc. Am.* **71,** 1249–1268.

Menke, W. (1989). *Geophysical Data Analysis: Discrete Inverse Theory*, Academic Press, San Diego, California.

Panning, M., D. Dreger, and H. Tkalčić (2001). Near-source velocity structure and isotropic moment tensors: a case study of the Long Valley caldera, *Geophys. Res. Lett.* **28,** 1815–1818.

Panza, G. F., and A. Saraò (2000). Monitoring volcanic and geothermal areas by full seismic moment tensor inversion: are non-double-couple components always artefacts of modeling? *Geophys. J. Int.* **143,** 353–364.

Prejean, S. G. (2002). The interaction of tectonic and magmatic processes in the Long Valley caldera, California, *Ph.D. Thesis*, Stanford University.

Prejean, S., W. Ellsworth, M. Zoback, and F. Waldhauser (2002). Fault structure and kinematics of the Long Valley caldera region, California, revealed by high-accuracy earthquake hypocenters and focal mechanism stress inversions, *J. Geophys. Res.* **107,** 2355, doi 10.1029/2001JB001168.

Roeloffs, E., M. Sneed, D. L. Galloway, M. L. Sorey, C. D. Farrar, J. F. Howle, and J. Hughes (2003). Water level changes induced by local and distant earthquakes at Long Valley caldera, California, *J. Volcanol. Geoth. Res.* **127,** 269–303.

Ross, A., G. R. Foulger, and B. R. Julian (1999). Source processes of industrially-induced earthquakes at The Geysers geothermal area, California, *Geophysics* **64,** 1877–1889.

Ryall, A. S., and F. D. Ryall (1984). Shallow magma bodies related to lithospheric extension in the western Great Basin, western Nevada and eastern California, *Earthquake Notes* **55,** 11–12.

Sanders, C. O., and L. D. Nixon (1995). S wave attenuation structure in Long Valley caldera, California from three-component S to P amplitude ratio data, *J. Geophys. Res.* **100,** 12,395–12,404.

Saraò, A., G. F. Panza, E. Privitera, and O. Cocina (2001). Non-double-couple mechanisms in the seismicity preceding the 1991–1993 volcano eruption, *Geophys. J. Int.* **145,** 319–335.

Sieh, K. E. (1984). Most recent eruptions of the Mono Craters, eastern California, in *Proceedings of Workshop. XIX: Active Tectonic and Magmatic Processes Beneath Long Valley Caldera*, *Eastern California*, *U.S. Geol. Surv. Open-File Rept. 84-939*, 96–129.

Šílený, J., P. Campus, and G. F. Panza (1996). Seismic moment tensor resolution by waveform inversion of a few local noisy records—I. synthetic tests, *Geophys. J. Int.* **126,** 605–619.

Steck, L. K., and W. A. Prothero (1994). Crustal structure beneath Long Valley caldera from modeling of teleseismic P-wave polarizations and P_s converted waves, *J. Geophys. Res.* **99,** 6881–6898.

Wallace, T.C. (1985). A reexamination of the moment tensor solutions of the 1980 Mammoth Lakes earthquakes, *J. Geophys. Res.* **90,** 11,171–11,176.

Berkeley Seismological Laboratory
215 McCone Hall, UC Berkeley
Berkeley, California 94720-4760